Structural Mechanics Optimization of the AISHa Ion Source

†*F. Noto¹, L. Andò¹, L. Celona¹, F. Chines¹, G. Ciavola¹,³, G. Costa¹, S. Gammino¹, O. Leonardi¹, S. Marletta¹, D. Nicolosi¹, G. Torrisi¹.²

¹ INFN - Laboratori Nazionali del Sud,Via S. Sofia 62, 95125 Catania, Italy
²Università Mediterranea di Reggio Calabria, Dipartimento di Ingegneria dell'Informazione, delle Infrastrutture e dell'Energia Sostenibile, Via Graziella, 89100 Reggio Calabria, Italy;
³ CNAO Foundation, Strada Campeggi, 53, Pavia PV, Italia

*Presenting author: francesco.noto@lns.infn.it †Corresponding author: francesco.noto@lns.infn.it

Introduction

Different facilities for hadron therapy have been built or designed in the recent past and Italy is present in the field either with synchrotron-based and with cyclotron-based facilities. For both types of accelerators the availability of high brightness multiply charged ion beams is essential and R&D efforts in this subject are increasing. In order to cope the stringent requests of a hospital environmental at INFN-LNS a new ion source called AISHa is under realization exploiting all the knowledge acquired in last decades in the ion source design and realization.

Therefore, the AISHa source has been designed by keeping in mind the typical requirements of hospital-based facilities, where the minimization of the mean time between failures (MTBF) is a key point together with the maintenance operations, which should be fast and easy. Some critical parts of the body source, in particular the plasma chamber and the hexapole containment chamber, have been studied and optimized with FEM softwares.

In the paper, the entire structure will be described, with a particular attention to thermomechanical simulations of the plasma chamber and the electrostatic and structural simulation of the hexapole containment chamber.

Keywords: Computation, Hadron Therapy, Ion Source, FEM, CFD

Introduction

The INFN-LNS has a broad experience in the design, construction and commissioning of ECR and microwave ion sources. In particular, since the '90s two sources for highly charged ion beam production, named SERSE and CAESAR, are operational to provide the heavy ions to be accelerated by the LNS K-800 Superconducting Cyclotron [1,2]The AISHa ion source has been designed by taking into account the typical requirements of hospital-based facilities, where the minimization of the mean time between failures (MTBF) is a key point together with the maintenance operations which should be fast and easy. [1,2]Therefore, a so called 3rd generation ECR ion source is not suitable, being quite complex for unskilled operators.

The new AISHa source is designed to be an intermediate step between the 2nd generation ECRIS (unable to provide the requested current and/or brightness) and the 3rd generation ECRIS [1] (too complex and expensive). It is intended to be a multipurpose device, operating at 18 GHz, in order to achieve higher plasma densities. It should provide enough versatility for future needs of the hadron therapy, including the ability to run at larger microwave power to produce different species and highly charged ion beams. At the same time, the electrical power to be installed for its operation will be kept below 50 kW. This demand implies also the simplification of all ancillary systems including an oven for metallic ion beams, which permits the

production of new beams for hadron therapy and for other applications.[2,3] The AISHa source (figure 1) is funded within the framework of the program of Sicilian Government named PO FESR 2007-2013 and a pool of Sicilian SME is associated with INFN for this project. The source is potentially interesting for any hadrontheraphy center using heavy ions.



Figure 1: Layout of the AISHa source

Mechanical development

In order to minimize the maintenance operations, the development of this new source involved some mechanical and structural improvements with respect to similar devices. In particular hereinafter the optimization of the hexapole containment chamber and of the source plasma chamber are described.

Use of COMSOL Multiphysics

The Finite Element Method approximates a Partial Differential Equations problem with a discretization of the original problem based on a mesh, which is a partition of the geometry into small units of simple shape called mesh elements. The PDE method looks for a solution in the form of a piecewise polynomial function, each mesh element defining the domain for one "piece" of it. Such a piecewise polynomial function will be expressed as a linear combination of a finite set of predefined basis functions. Let us consider for example a 2-dimensional problem with a single dependent variable p(x,y). The solving method implemented in this code is based on a mesh with quadratic triangular elements. The expression "quadratic elements" refers to the fact that on each mesh element the sought piecewise polynomial function p*(x,y) is at most a quadratic polynomial. In this case, the solution is expressed as:

$$p(x,y) \cong p^*(x) = \sum_{i=1}^n p_i \varphi_i(x,y)$$

where *i* refers to a node of the mesh, pi are the degrees of freedom, $\varphi_i(x,y)$ are the basis functions and n is the total number of nodes, under the assumption that each triangle of the mesh possesses six nodes: three corner nodes and three mid-side nodes [4]. A basis function $\varphi_i(x,y)$ has here the restriction to be a polynomial of degree at most 2 such that its value is 1 at node *i* and 0 at all other nodes [5]. The degree of freedom pi is thus the value of p*(x,y) at node *i*. The definition of the basis function associated to each node

of the mesh can be derived using for example a general method introduced by Silvester in 1969 [6].

COMSOL's Thin-Film Flow Model for optimitation plasma chamber

All of COMSOL's single-phase fluid flow interfaces are based on the three fluid dynamics conservation equations known as the Navier-Stokes equations [4], concerning the conservation principles of mass, momentum and energy (Figure 2):

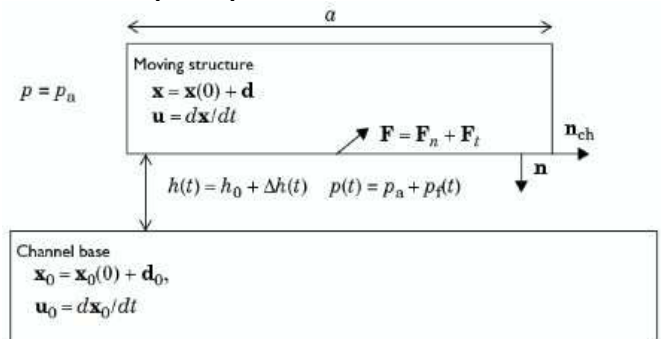


Figure 2. Schematic diagram of the situation to which the thin-Film Flow Model applies

The model that has been used in our simulations is the Thin-Film Flow Model [7] and belongs to the Computational Fluid Dynamics (CFD) module. The Thin-Film Flow Model can be used to model a thin channel fluid located between two moving structures, as schematized in Figure 2. The upper structure is referred to as the moving structure and the lower one as the channel base. Initially, both structures are surrounded by gas with a constant pressure p_a and the fluid can freely move into and out of the gap. Due to the movements of the structures, an additional and usually time-dependent pressure p_f appears in the gas inside the gap, which produces a normal force $\overline{F_n}$ on the structures. Also a viscous drag force $\overline{F_t}$ is created which resists the tangential movement of the structure. In the Thin-Film Flow Model, it is however assumed that:

- The film thickness h remains always very small with respect to the dimensions of the solid structures.
- The channel curvature is small.

Also the following assumptions are made:

- The inertial effects in the fluid are negligible compared to the viscous effects, thus the flow is laminar.
- The pressure $p = p_a + p_f$ is constant over the film thickness h.
- The velocity profile over the film thickness is parabolic.
- The fluid is isothermal.

Given these assumptions, solving the fluid flow problem with the Navier-Stokes equations reduces to solving the following equation, called the Reynolds equation:

$$\frac{\partial (ph)}{\backslash} + \ \overrightarrow{\nabla}_{tg} \cdot (\rho h \overrightarrow{U}) - \rho (\overrightarrow{\nabla}_{tg} \Delta h_m \cdot u_m - \overrightarrow{\nabla}_{tg} \Delta h_b \cdot \overrightarrow{u_b}) = 0$$

where ρ is the density, $h = h_0 + \Delta h_m + \Delta h_b$ is the film thickness, t is the time, V_{tg} is a gradient computed only with the tangential derivatives along the channel boundaries, U is the mean film velocity, Δh_m and u_m are the normal displacement and the tangential velocity of the so-called "moving structure", respectively, and Δh_b and u_b are the normal displacement and the tangential velocity of the "channel base", respectively. The mean film velocity U is actually a function of the pressure p, the dynamic viscosity μ , the film thickness h, the tangential velocities u_m and u_b of the solid structures and the relative flow rate function Q_{ch} that accounts for possible rarefied gas effects:

$$\vec{U} = \frac{\vec{\nabla}_{tg} \, p}{12\mu} h^2 Q_{ch} + \frac{u_m + u_b}{2}$$

Permanent water flow in the plasma chamber is required to provide the expected low temperature. [9] Therefore, the goal of our study was to optimize the design of the groove. This optimization of the particular was done starting from a model of the chamber used in other sources. The model was designed considering four cylinders: $\varphi = 92$ mm (chamber inner diameter), $\varphi = 94$ mm (water flow internal diameter), $\varphi = 102$ mm (water flow outside diameter) and $\varphi = 104$ mm (chamber external diameter), each divided in two half cylinders. For each of the two half-cylinders an input, an output and three septa were designed. The domains considered were two, one for water and one for the metal (AISI 316L and aluminum 3003-H18) (Figure 3).

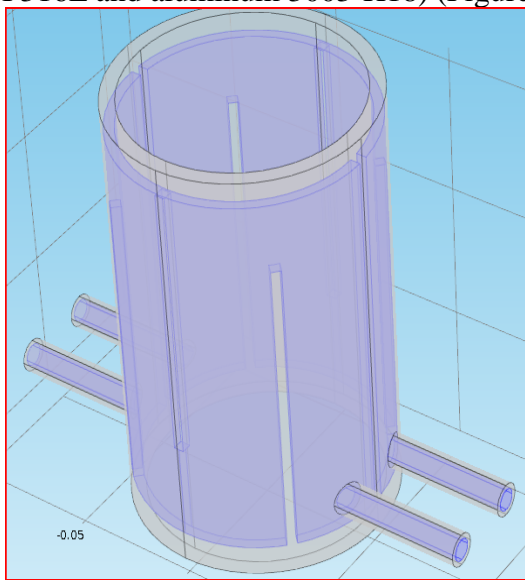


Figure 3. The first model, in gray the metal domain and in purple the water domain.

For the inlet an initial velocity of the water has been determined by requiring a flow rate of 3 liters / minute (0.00005 m³/s) and calculating the section of the input (the input to the diameter is 4 mm so the area is 0.0000502 m²). From the relation:

$$v = \frac{Q}{A} \tag{1}$$

by substituting the calculated values we obtain that the initial speed has to be 1 m/s. The initial water temperature was set at 20 $^{\circ}$ C.

Concerning the mesh, for both domains we have chosen a tetrahedral mesh. In the domain of the water the choice was to use a mesh more dense than in the domain of the metal. The results obtained in the case of aluminum 3003-H18 show that the temperature reaches the maximum value of about 300 °K at the output of water, that is, after the water has traveled the half cylinder, it is heated and has lost in part its cooling capacity. Nevertheless, this temperature is satisfactory, as we must have a maximum surface temperature of the lower chamber of 50°C in order not to damage the magnets that are in contact with it. The flow obtained is substantially laminar. Calculating the Reynolds number with the expression:

$$Re = \frac{v * D}{u} (2)$$

and assigning the values: v=0.35 m/s (the highest in the flow), D=0.004 mm and assuming the value $1.01*10^{-6}$ m²/s for the kinematic viscosity μ of the water, we get a Reynolds number equal to 1386 so we are in the field of laminar flow (Re less than 2300 is laminar flow) (Figures 4 and 5).

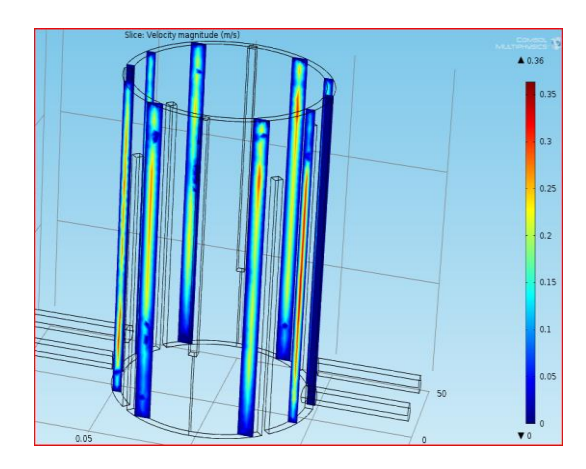


Figure 4. Velocity speed in the aluminum case.

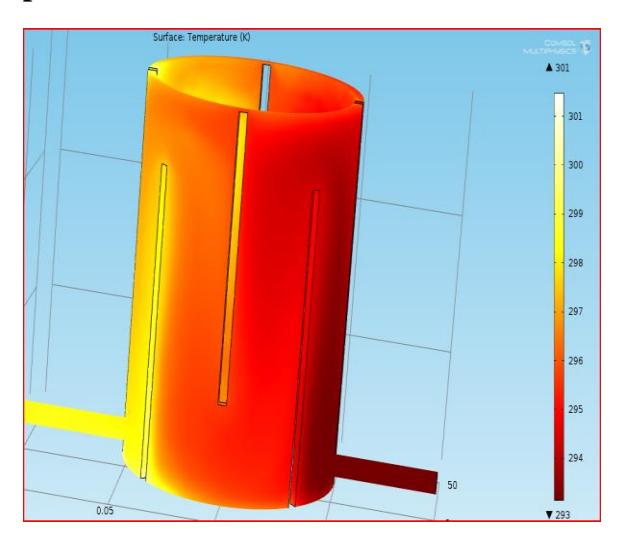


Figure 5. Temperature in the aluminum case. Subsequently the simulation has been developed using the AISI 316L steel as metal material. The results obtained for the velocity of the water are similar to the case of aluminum, while the maximum temperature reached is lower than in the previous case (Figure 6 and 7).

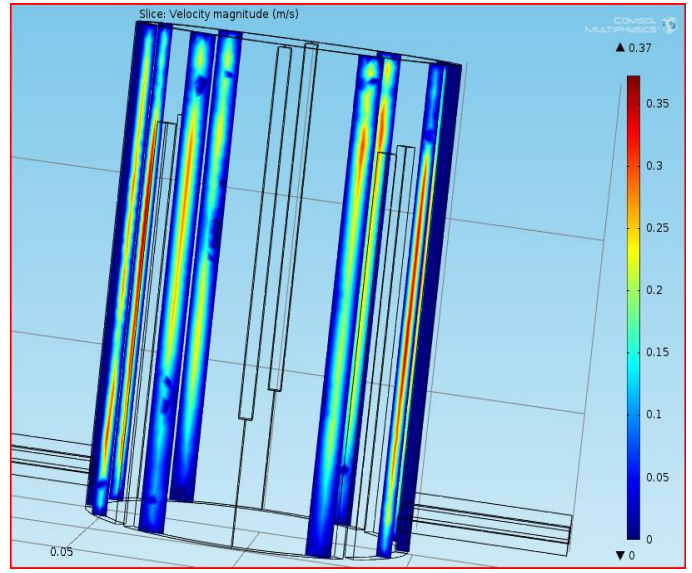


Figure 6. Velocity speed in the aluminum case.

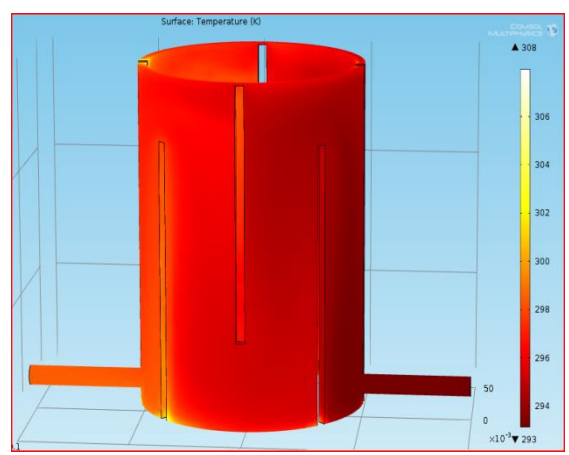


Figure 7. Velocity speed in the aluminum case.

This temperature decrease is due to the characteristics of the two materials: in fact the thermal conductivity of steel (14.6 W/m*K), is lower than that of aluminum (155 W/m*K); it is a measure of the ability of a material to transmit heat (i.e. the lower the value of k, the more insulating is the material).

The first step has been developed using the COMSOL code, considering a length of the chamber of 155 mm. Then the simulation was performed for the actual size of the chamber, that is 655 mm, but as the plasma formation takes place within 360 mm it has been decided to simplify the simulation, and then the calculations, considering a total length of 360 mm. Another simplification was to divide the plasma chamber into 4 equal sectors each with an input and an output (Figures 8, 9, 10).

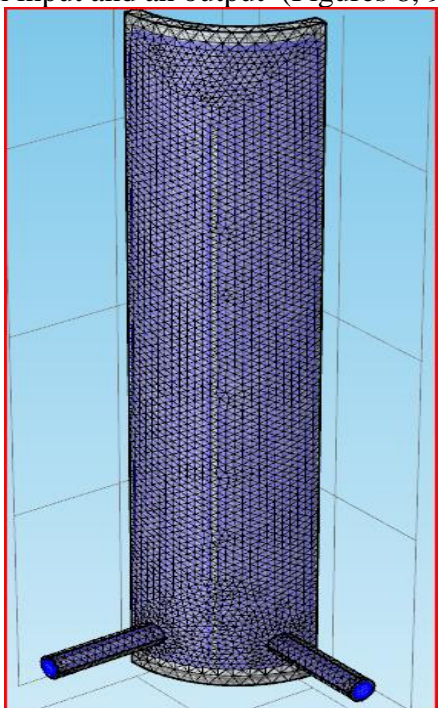


Figure 8. The mesh in the new model

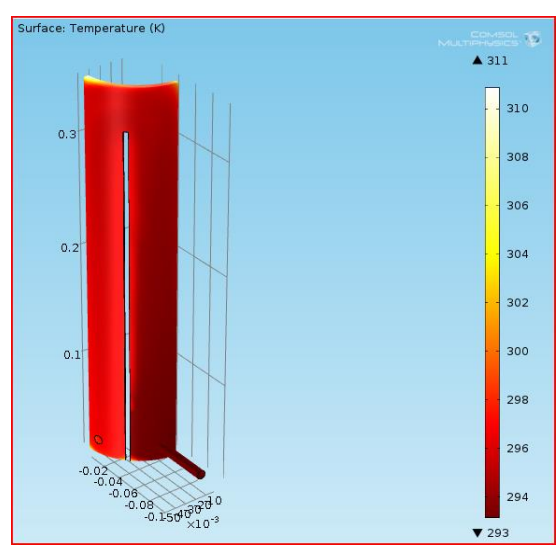


Figure 9. The temperature values in the AISI 316L case.

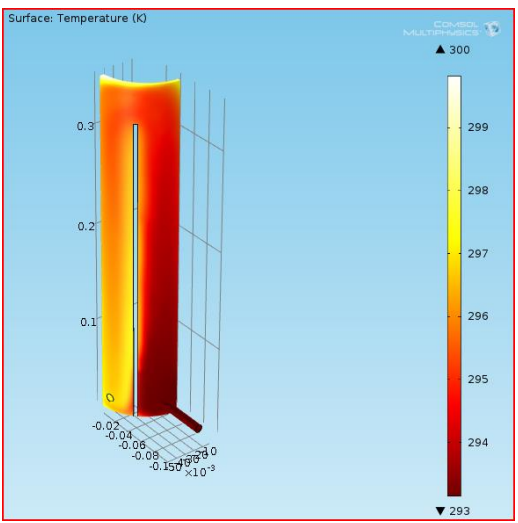


Figure 10. The temperature values in the aluminum 3003-H18 case

An interesting detail is that the D_t between a point near the entrance and a point near the water outlet is about 4°C and the average temperature is 24 °C. The maximum temperature of 38 °C is on edge (not influential value) as shown in Figure 11a and 11b.

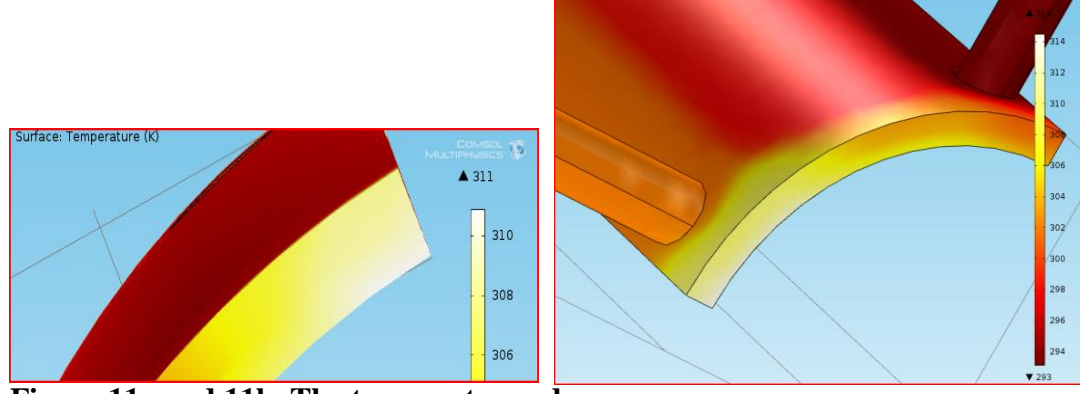


Figure 11a and 11b. The temperature edge.

As in step 1, we have developed the same simulations in the case of another metal material, aluminum 3003-H18.

The results obtained for the water velocity are quite similar to each other (Figure 12).

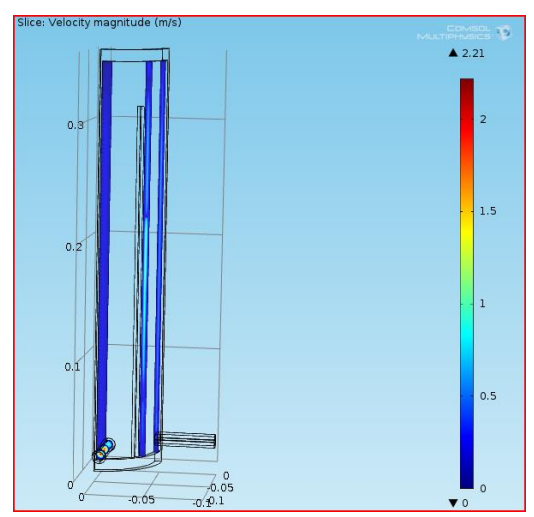


Figure 12. The water velocity values in the aluminum 3003-H18 case

In the plasma chamber the speed values are on average equal to 0.5 m/s and therefore we are in laminar regime as the Reynolds number is about 2000.

Pressure drop was calculated using the expressions of both the distributed and concentrated losses. The former is:

$$\Delta p = \rho * \xi * \frac{L}{D} * \frac{v^2}{2}$$
 (3)

where ρ is the density of water, ξ is the friction factor calculated by means of the Moody (using the Reynolds number and the roughness of the material), L is the length of the chamber, D the diameter of the duct of water (assumed in this case a size of the water domain equal to 4 mm) and v the velocity of water (assumed an average speed of 0.5 m/s from the simulation): the calculation leads to a D_p of about 0.01 bar. For concentrated losses the expression is:

$$\Delta p = \beta * \rho * \frac{v^2}{2} \qquad (4)$$

where ρ is the water density, β is the coefficient of friction equal to 0.5 for the 90-degree elbow and v is the velocity of the water in different cases. The calculation leads to a D_p of about 0.01 bar to the entrance (v = 2 m/s); D_p of about 0.002 bar for the output (v = 0.9 m/s) and D_p of about 0.0006 bar in the elbows due to the septum (v = 0.5 m/s): the sum of all the losses yields a loss of load of 0.023 bar.

Minimization of the stray magnetic field in the extraction area.

The AISHa magnetic field is provided by a set of four superconducting coils able to create a mirror field as shown in fig. 13 with respectively 2.7 T and 1.7 axial field at injection and extraction. The forces between the coils have been decreased to 30 tons for safe operation at maximum field, in this operating conditions different calculations have been performed to minimize the field in the extraction area to avoid unwanted effects on beam optics and to minimize sparks in the extraction gap.

In order to decrease the magnetic field in this area where the beam is formed an iron piece suitably shaped (see Figure 13) anchored to the extraction flange has been added. As you can see from Figure 14 the introduction of such workpiece produces a considerable increase of the gradient of the magnetic field which therefore decreases significantly in the extraction area for z> 240 mm.

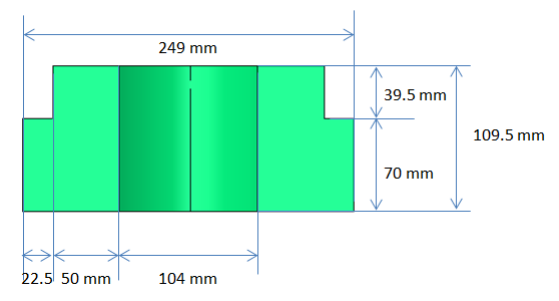
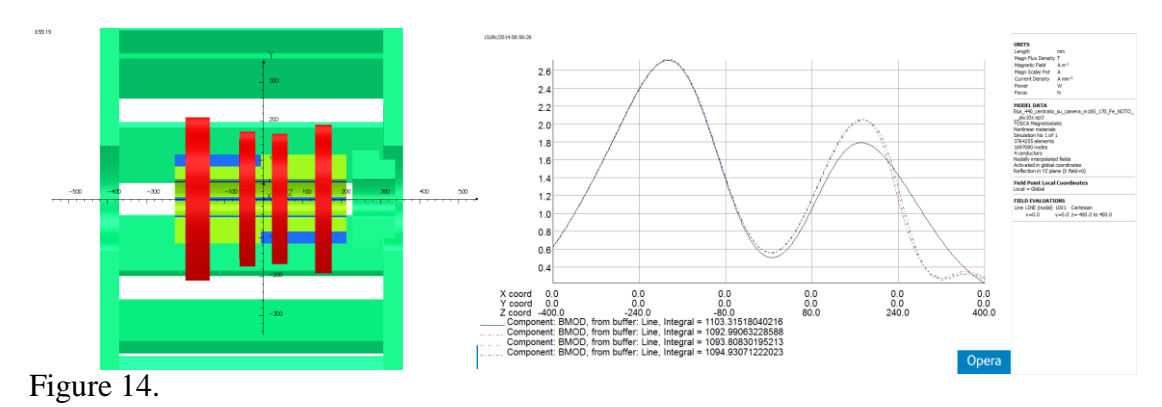


Figure 13. Iron add dimension



The presence of the added iron produces a negligible effect both to the hexapole magnetic field and to the force acting on the extraction coil. However, it is subject to a force superior to 6 tons and this can create problems anchoring, Figure 15 shows the force acting on the iron depending from its longitudinal direction, a possible choice was therefore to remove 25 mm of iron to achieve a force of 4.46 tons that can be easily contained.

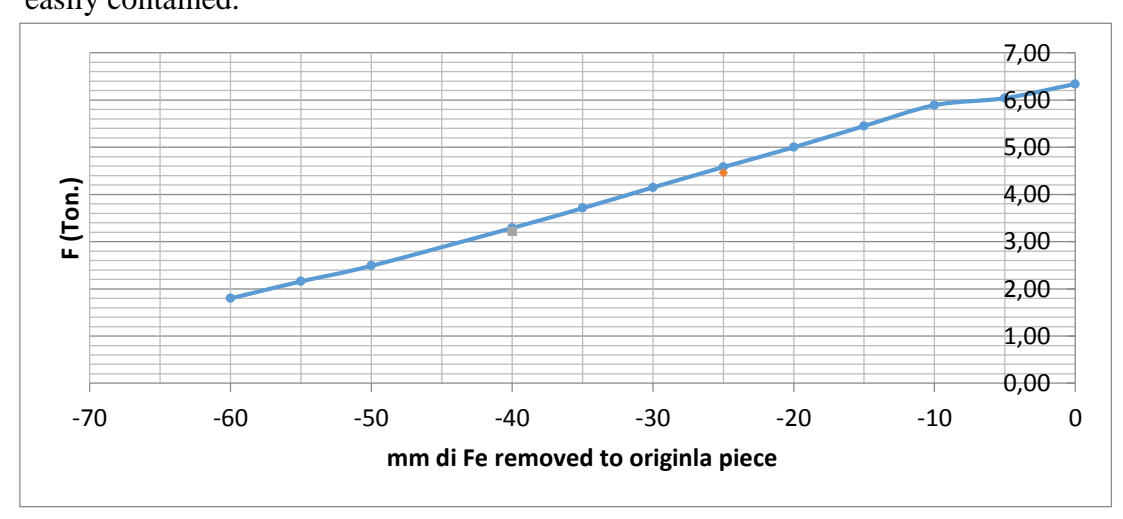


Table 1

Subsequently to further decrease both the weight and the force it was decided to remove up to 40 mm from the original part and arrive in this way to 3.3 tons of force, which decrease up to 2.2 ton increasing the holes diameter from 104 mm to 164 mm. (tab. 2 and fig 16).

Iron Add -40 mm	Force (ton.)
$\phi_{int} = 104 \text{ mm}$	3.29
$\phi_{int} = 114 \text{ mm}$	3.18
$\phi_{int} = 124 \text{ mm}$	3.07
$\phi_{int} = 134 \text{ mm}$	2.92
$\phi_{int} = 144 \text{ mm}$	2.72
$\phi_{int} = 154 \text{ mm}$	2.49
$\phi_{int} = 164 \text{ mm}$	2.20
$\phi_{int} = 174 \text{ mm}$	1.89
$\phi_{int} = 184 \text{ mm}$	1.52

Table 2. Force variation function of the diameter variation.

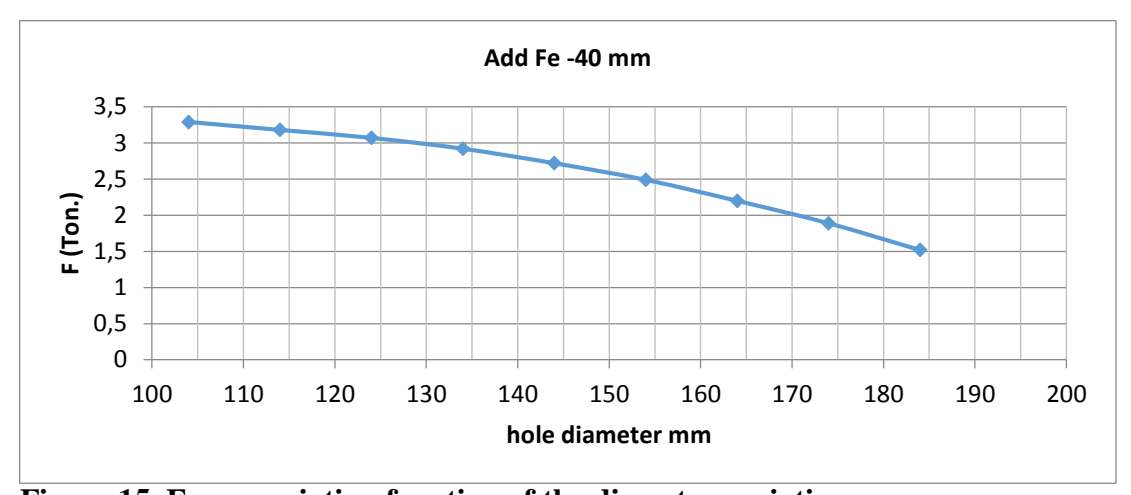


Figure 15. Force variation function of the diameter variation.

This configuration, albeit even if mechanically valid, was discarded due to static problems, in fact there discharges may occur due to the iron shape, therefore it was decided to change their profile (figure 16) and see the table 3.

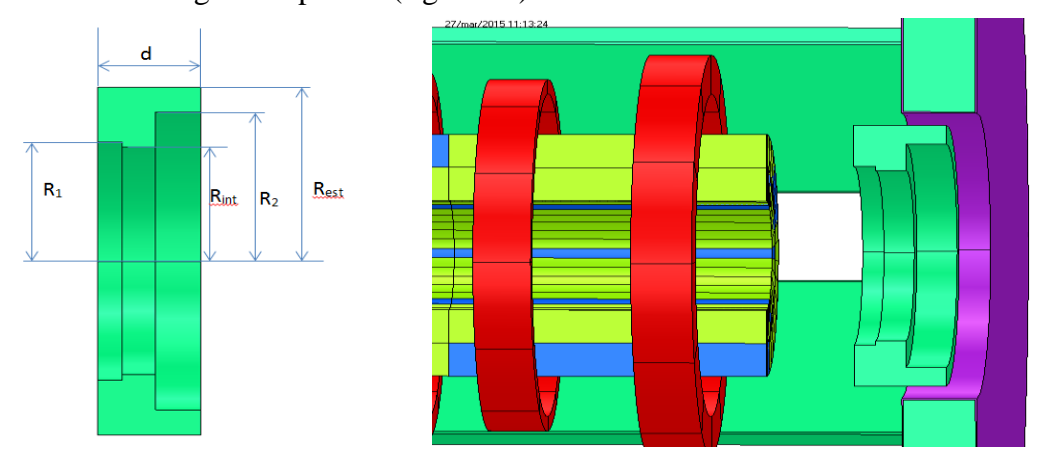


Figure 16a and 16b. New profile and iron parte in loco

	d	Rint	R_1	R_2	Rest
Fe1	64	81	85	106	124
Fe2	74	81	85	106	124
Fe3	84	81	85	106	124
Fe4	94	81	85	106	124

Table 3. Size variations of particular "added iron"

In the framework of pressure vessels, the threaded connections are used to connect the cover to the body of the containers, or to connect two pipe sections etc. However, the speech fact also applies to other cases. On the two the endpoints of the pipe to be connected are welded two flanges between which is interposed a more yieldable gasket material which serves to ensure the sealing.

At first the screw are tightened to ensure sealing; then the container is pressurized. To effect of the pressure screws are stretched further, while the gasket is download. However, a certain load must stay on it to prevent leakage.

In the phase of pre-tensioning the bolts are stretched by a total force W_I and correspondingly the seal is compressed by a force $-W_1$.

In the step of pressurizing the internal pressure p causes the onset of the force W_2 = $\frac{\pi G^2 p}{4}$ where G is the mean diameter of gasket; this causes a shift δ_2 upwards cover compared to the coat. Correspondingly, screws stretch of δ_2 and gasket it increases its thickness δ_2 .

 K_b are the force that causes a lengthening unit of the screws (stiffness of the screws) kg the force which causes a decrease of unitary gasket thickness (stiffness of the gasket).

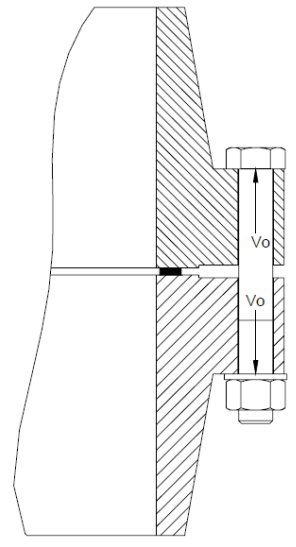


Figure 17. Flange connection between mantle and cover

To create the screws axial load W_1 calculated in the previous section (ie a load of W_1/N on each screw) must tighten the nuts with the proper tightening torque (popularly called tightening torque).

To calculate this we observe that the torque screw-nut screw is dynamically equivalent to a inclined plane. When the nut rotates in the the screwing element is brought from the position 1 to position 2 for example. To make this shift must be a force dT perpendicular to the axis screw.

For the balance, and considering that all elements are in the same condition

$$T = \frac{W_1}{N} \tan(\alpha + \varphi)$$

Where the α helix angle of the thread for a screw with pitch p and φ friction angle. So

$$M_t = \frac{D_m}{2} \frac{W_1}{N} \tan \varphi'$$

 $M_t = \frac{D_m}{2} \frac{W_1}{N} \tan \varphi'$ where φ ' angle of friction between the nut and the bearing surface and D_m is the mean diameter of the nut (average width between key and nominal diameter). The tightening torque is given by the sum of these two partial moments of which the second is

completely lost, while the first remains stored in screw as torque. Applying these calculations to our system, or the closing flange between the yoke and the plasma chamber and considering our values namely a diameter of 250 mm we obtain that the minimum number of screws is 12 and with a pressure of 30000 N/cm it is obtained that the minimum diameter of the life to be applied is a M14 with a minimum length of 35 mm. It was subsequently also set a finite element simulation to check the tightness of the flange with the assumptions made and the results obtained show that the theoretical calculations made were correct and the maximum displacement is $1.08 \times 10_{-5}$ m (figure).

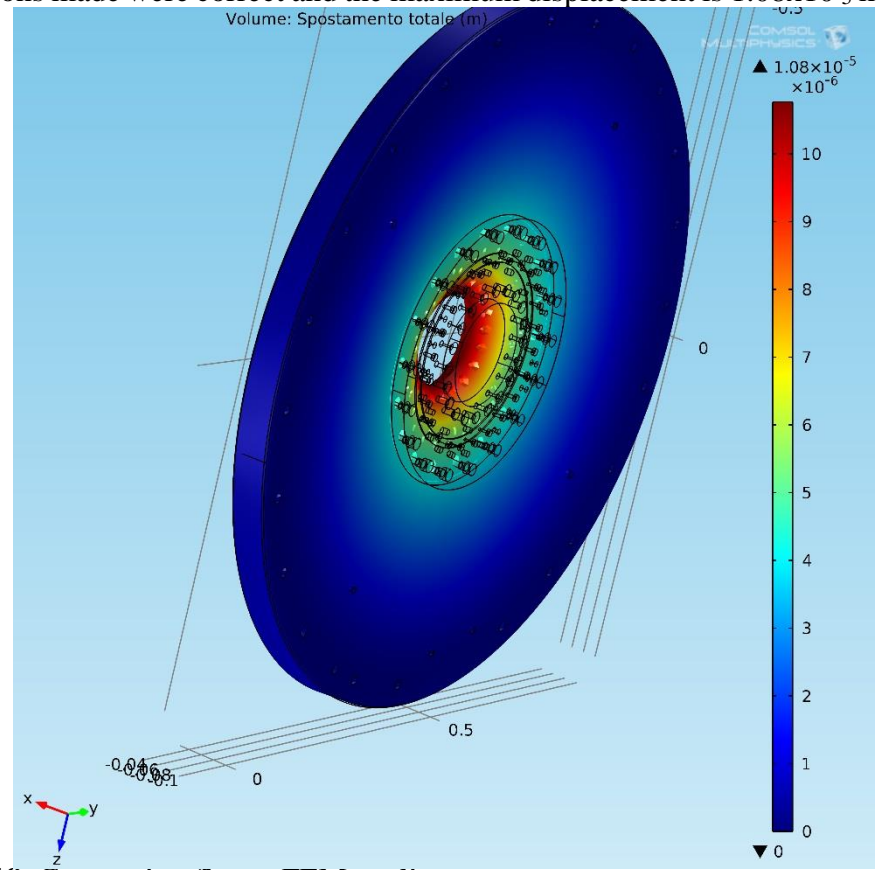


Figure 18. Connection flange FEM analisys

Conclusions

The optimization of the AISHa plasma chamber design and all mechanical parts have been pursued with FEM codes.[8] The parts are currently under construction and the source will be assembled in next September at INFN-LNS.

References

- [1] L. Celona, G. Ciavola, S. Gammino, L. Andò, D. Mascali DESIGN OF THE AISHA ION SOURCE FOR HADRON THERAPY FACILITIES Proceedings of ECRIS2012, Sydney, Australia, ISBN ISBN 978-3-95450-123-654
- [2] S. Gammino et al., Rev. Sci. Instrum. 70, 9 (1999), 3577
- [3]. S. Gammino, G. Ciavola, Rev. Sci. Instrum. 71, 2 (2000), 631
- [4] Felippa C.A., Introduction to Finite Element Methods, lecture notes, Department of aerospace engineering sciences of the University of Colorado, Boulder, 2004.
- [5] COMSOL Multiphysics User's Guide v4.1, COMSOL A B, 2010.
- [6] Lewis R.W., Nithiarasu P. & Seetharamu K.N., Fundamentals of the Finite Element Method for Heat and Fluid Flow, New York, John Wiley & Sons, 2004.

- [7] CFD Module User's Guide v4.1, COMSOL AB, 2010.
- [8] L. Celona et al. ECR IONS SOURCE DEVELOPMENT AT INFN-LNS Proceedings of ECRIS2014
- [9] F. Noto et al, Optimization of the gas flow in a GEM Chamber and development of the GEM foil Stretcher Nuclear Technology & Radiation Protection, 2014, vol.29 suppl, pp s0-s0, DOI: 10.2298/NTRP140202?N